Geophysical Journal International

Geophys. J. Int. (2024) **236,** 1753–1763
Advance Access publication 2024 January 15
GJI Applied and Marine Geophysics

https://doi.org/10.1093/gji/ggae020

Stress and frequency dependence of wave velocities in saturated rocks based on acoustoelasticity with squirt-flow dissipation

Jing Ba,[1,2] Yijun Wei,[1,2] José M. Carcione,[3] Ludmila Adam[2] and Genyang Tang[4]

[1]*School of Earth Sciences and Engineering, Hohai University, Nanjing* 211100, *China. E-mail: yijun@hhu.edu.cn*
[2]*School of Environment, University of Auckland, Auckland* 1010, *New Zealand*
[3]*National Institute of Oceanography and Applied Geophysics - OGS, Trieste* 34010, *Italy*
[4]*College of Geophysics, China University of Petroleum (Beijing), Beijing* 102249, *China*

Accepted 2024 January 13. Received 2024 January 7; in original form 2023 October 12

SUMMARY

We perform seismic and ultrasonic measurements in carbonate and shaley sandstone samples as a function of differential pressure. The velocities show a strong frequency and pressure dependence. The dispersion disappears with increasing pressure and the squirt flow in turn inhibits the pressure dependence. To model these effects, we combine the Gurevich's squirt-flow model with the Mori–Tanaka scheme and the David Zimmerman model, and extend it with third-order elastic constants, to obtain a frequency-dependent acoustoelasticity model. Comparisons between measurements from this study and literature and modelling results show that the *P*-wave velocity increases non-linearly first and then nearly linearly, dominated by crack closure and acoustoelasticity, respectively. The pressure dependence of wave velocities is reduced by liquid substitution and further by the squirt-flow mechanism. The effects of fluid properties and crack closure on *P*-wave velocity decrease with differential pressure. The results will feed a new model and help better understanding the wave propagation in pre-stressed rocks at different scales.

Key words: Fracture and flow; Permeability and porosity; Wave propagation; Microstructures; Acoustic properties.

1 INTRODUCTION

In fluid-saturated porous rocks, the acoustic wave properties are affected by the pressure-dependent pore structure as well as by the pore fluid in a wide range of frequencies (White 1975; Winkler 1985; Wang & Nur 1990; Pride *et al.* 2003, 2004; Wang *et al.* 2012). Extensive research has dealt with wave-induced squirt-flow loss in fluid-saturated media (Murphy *et al.* 1986; Mavko & Jizba 1991; Dvorkin & Nur 1993; Dvorkin *et al.* 1995; Gurevich *et al.* 2009, 2010). Despite the frequency dependence of second-order elastic moduli at low differential pressures, the prediction is successful using classical squirt-flow models. However, these models do not adequately describe the pressure-dependent wave velocities, as they neglect the stress-induced linear elastic deformation in stiff pores and aggregates, the so-called acoustoelasticity effect. The theory of acoustoelasticity introduces third-order elastic constants (3oEC) and finite strains to describe stress-dependent wave velocities in rocks (Jones & Kobett 1963; Brugger 1964; Green 1973; Meegan *et al.* 1993; Kravchishin & Chekurin 2009). Therefore, the coupling of wave velocity with frequency and pressure dependence is the central topic of this study.

Previous researches have shown considerable dispersion in acoustic wave velocity from seismic to ultrasonic frequency bands (Wyllie *et al.* 1958; Walsh 1965; Nur & Simmons 1969; Murphy 1982; Pimienta *et al.* 2015a,b; Chapman *et al.* 2016, 2019). The main cause of the dispersion is assumed to be wave-induced fluid flow, which can occur on several scales. On the wavelength scale, global flow dispersion arises from the motion of the fluid relative to the solid frame, driven by the pressure gradients between the peaks and troughs of the passing wave (Gurevich *et al.* 2010; Alkhimenkov *et al.* 2020). On the mesoscopic scale, the flow between patches resulting from rock heterogeneity or spatial variations in fluid saturation can be described by Biot's theory (Biot 1956, 1962; Pride *et al.* 2004). At the pore scale, local fluid movement (also known as squirt flow) occurs between regions of different compliances (Winkler 1985; Batzle *et al.* 2006; Müller *et al.* 2010; Tisato *et al.* 2021). The fluid in the pores may exhibit stiffer elastic behaviour in the high-frequency band as if the pores were completely isolated (David *et al.* 2013).

Extensive experimental studies have shown a non-linear increase in velocity with differential pressure (Walsh 1965; Khaksar *et al.* 1999; Smith *et al.* 2010; Pimienta *et al.* 2015b, 2016). Smith *et al.* (2010) attributed this trend to the double-porosity structure in rocks,

particularly in the presence of compliant pores (cracks). Shapiro (2003) reported that the greater the crack porosity, the greater the elastic non-linearity of rocks. The effect of crack closure dominates the non-linear increase in the second-order elastic constants (moduli) of the dry rock with the increasing differential pressure. The velocity increases almost linearly at the high-pressure end due to the near complete closure of cracks and the finite deformation of stiff pores and grains (Fu & Fu 2018).

A number of models describing the squirt-flow mechanism between stiff pores and cracks have been proposed to simulate wave-induced fluid flow at the pore level (Murphy *et al.* 1986; Dvorkin & Nur 1993, 1995; Tang 2011). Mavko & Jizba (1991) quantified the effect and derived the unrelaxed bulk and shear moduli of fluid-saturated rock; however, the result is not applicable to low-moduli fluids, such as light gas. Gurevich *et al.* (2010) modified the moduli based on the Sayers–Kachanov discontinuity formalism for a rock saturated with a fluid of arbitrary bulk modulus (see also Carcione & Gurevich 2011; Gurevich & Carcione 2022). Han *et al.* (2018) showed that this model has good agreement with experimental data at low confining stresses, but underestimates wave attenuation at high pressures. Alkhimenkov *et al.* (2020) evaluated Gurevich's model and concluded that it is accurate for a stiff porosity of zero, but inaccurate for a non-zero stiff porosity, as the influence of the connectivity of cracks and stiff pores is not considered. Alkhimenkov & Quintal (2022) improved the squirt-low model of Gurevich *et al.* (2010) for isotropic rocks.

Acoustoelasticity, established within the hyperelasticity framework, describe the stress-induced finite elastic deformation and higher-order elasticity in pure solid, which can be modelled with 3oEC (Hughes & Kelly 1953). This theory can explain stress-induced velocity changes (Jones & Kobett 1963; Green 1973; Meegan *et al*. 1993). Hughes & Kelly (1953) derived expressions of stress-dependent wave velocities by using Murnaghan's finite deformation theory and estimated three 3oEC, denoted as *l*, *m* and *n*. Winkler & Liu (1996) measured the 3oEC, which describes well the velocities as a function of stress in dry rocks. However, classical acoustoelasticity theory cannot explain the measurements in saturated rock (Winkler & McGowan 2004). The theory has been further extended to a fluid-saturated porous solid (Biot 1973; Ba *et al.* 2013), but the models do not account for the effects of non-linear deformation of cracks (Fu & Fu 2018) and squirt flow.

In this work, we complement the Gurevich's squirt-flow model with the Mori–Tanaka scheme of effective medium theory and integrate 3oEC to derive a frequency-dependent acoustoelasticity model. We measure seismic and ultrasonic *P*- and *S*-wave velocities at different differential pressures in a shaly sandstone sample. By comparing theoretical predictions with measurements and test data reported in the literature, we analyse the effects of pressure-induced changes in pore structure and rock framework, as well as frequency dependence associated with squirt flow, on wave propagation in saturated rock. The present model allows for a useful tool to characterize the pressure-dependent elastic properties at different frequencies, which will contribute to geofluid detection, crack identification and reservoir exploitation by translating the differential pressure into depth of seismic field data.

2 THEORY

2.1 Poroelasticity with squirt-flow dissipation

When acoustic waves propagate through a fluid-saturated medium, soft pores/cracks are squeezed by the waves and tend to deform more than stiff pores, resulting in an internal pressure gradient of the pore fluid. Squirt flow occurs when energy is dissipated until fluid pressure equalises (Paula *et al.* 2012). Fig. 1 illustrates the stress- and frequency-induced changes in pore structure of dry (or gas-saturated, where the bulk modulus of the fluid is negligible) and saturated rock. In saturated rock, the pressure of the pore fluid has sufficient time to reach equilibrium in the squirt flow between pores and cracks within half a wave cycle (i.e. in a relaxed state) in the low frequency range. At intermediate frequencies, the fluid pressure gradually shifts to a partially unrelaxed state and stiffens the rock framework, causing wave dispersion. When the wave frequency is higher than the characteristic squirt-flow frequency, the pore fluid and rock framework approach the unrelaxed state (Mavko & Nur 1975, 1979). To describe the frequency dependence of elastic moduli, Gurevich *et al.* (2010) presented a squirt-flow model, such that the reciprocal of the modified rock frame (mf) with liquid-saturated cracks and dry stiff pores, is

$$\frac{1}{K_{mf}} = \frac{1}{K_h} + \left(\left(\frac{1}{K_m} - \frac{1}{K_h} \right)^{-1} + \left(\left(\frac{1}{K_f^*} - \frac{1}{K_g} \right) \phi_c \right)^{-1} \right)^{-1} \tag{1a}$$

$$\frac{1}{\mu_{mf}} = \frac{1}{\mu_m} - \frac{4}{15} \left(\frac{1}{K_m} - \frac{1}{K_{mf}} \right), \tag{1b}$$

where K and μ are the second-order bulk and shear moduli, respectively. Subscripts g, h and m refer to grain (mineral), dry-rock frame with only stiff pores and dry-rock frame with stiff pores and cracks, respectively. ϕ_c is crack porosity. Moreover, $K_f^* = [1 - 2J_1(ka)/(kaJ_0(ka))]K_f$ is the effective bulk modulus of the modified fluid, where $ka = [-3i\omega\eta/(\alpha_c^2 K_f)]^{1/2}$, k is the wavenumber of the pressure diffusion wave in a crack with radius a, K_f and η are the bulk modulus and viscosity of pore fluid, respectively, J_1 and J_0 denote the Bessel equations of zero order and first order, respectively, and ω is the angular frequency. In addition, α_c is the minimum value of the initial aspect ratio of those cracks which are still open at a given pressure.

The squirt-flow effect depends on the pore geometry and the roughness of the cracks, especially on the presence of open cracks or grain contacts (Pimienta *et al.* 2016; Lissa *et al.* 2020). Once the differential stress–pressure is high enough for the cracks to approach closure and no soft pores are available for squirt flow to occur (Fig. 1), the effect disappears (Han *et al.* 2018). To determine the moduli of the effective dry-rock frame in terms of crack parameters, the Mori–Tanaka scheme of effective medium theory (Mori & Tanaka 1973) and the David-Zimmerman model (David & Zimmerman 2012) are applied.

For a dry or light gas-saturated rock (Fig. 1), high compressibility permits pore fluid pressure equilibrium (Batzle *et al.* 2006) and wave anelasticity–dispersion are negligible (David *et al.* 2013). The pressure dependence is related to the variations in a double-porosity structure consisting of pores and cracks (Shen *et al.* 2020). According to the Mori–Tanaka scheme (Mori & Tanaka 1973), the effective second-order bulk and shear moduli of dry rock are, respectively,

$$K_m = K_h \Big/ \left(1 + \frac{16\left(1 - (\nu_h)^2\right)\rho_c}{9\left(1 - 2\nu_h\right)} \right), \tag{2a}$$

$$\mu_m = \mu_h \Big/ \left(1 + \frac{32\left(1 - \nu_h\right)\left(5 - \nu_h\right)\rho_c}{45\left(2 - \nu_h\right)} \right), \tag{2b}$$

where ν_h=$(3K_h - 2\mu_h)/(6K_h + 2\mu_h)$ is the stiff-pore Poisson ratio (cracks closed), and ρ_c is the cumulative crack density (total number of cracks embedded within a unit volume). If the crack parameters

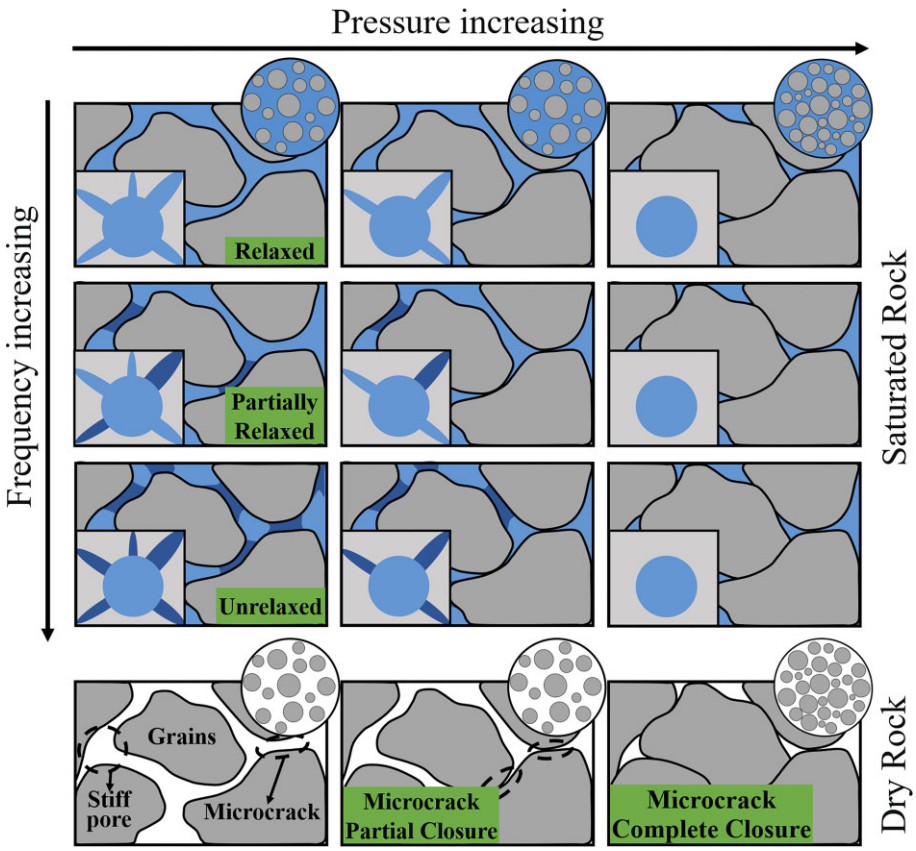

Figure 1. Diagram of the structural changes of the dry and saturated rock as a function of differential pressure. The squirt flow is inhibited with increasing pressure and frequency,. The circular and square insets indicate the acoustoelasticity and squirt-flow mechanisms, respectively.

are known, it is possible to estimate the dry-rock wave velocities and vice versa.

David & Zimmerman (2012) propose the following empirical relation between crack density and differential pressure σ as

$$\rho_c = \rho_{\rm ci} e^{-\sigma/\hat{\sigma}}, \tag{3}$$

where $\rho_{\rm ci}$ is the initial crack density and $\hat{\sigma}$ is the compaction coefficient that characterizes the rate at which the compliances level off.

The relation between the crack aspect ratio and differential pressure is (David & Zimmerman 2012)

$$\alpha_c = \frac{4\left[1-(\nu_h)^2\right]\sigma}{\pi E_h}, \tag{4}$$

where $E_h = 3K_h[1-2\nu_h]$ is the stiff-pore Young modulus.

The relation between crack density and crack porosity is (Vernik & Kachanov 2010; David & Zimmerman 2012)

$$\phi_c = \frac{4\pi\alpha_c}{3}\rho_c. \tag{5}$$

By substituting the crack parameters and second-order moduli into eq. (1), the squirt-flow model for a saturated rock with pores and cracks is obtained.

2.2 Acoustoelasticity

2.2.1 Classical theory

The squirt-flow model of Section 2.1 accounts for pressure relaxation due to the double-porosity structure, which allows for frequency-dependent elastic moduli. While the cracks gradually close with increasing pressure, the wave velocity increases almost linearly due to the close grain-to-grain contacts and finite deformation. This is known as the acoustoelasticity effect (Biot 1973; Fu & Fu 2018), but it is currently ignored in the squirt-flow model. The classical acoustoelasticity theory introduces 3oEC to describe the stress-induced finite deformations in the solid and the corresponding wave velocity changes (Murnaghan 1937; Hughes & Kelly 1953),

$$\rho V_P^2 = \left(K_h + \frac{4}{3}\mu_h\right) - \frac{\sigma}{3K_h}\left(7K_h + \frac{16}{3}\mu_h + 6l_h + 4m_h\right), \tag{6a}$$

$$\rho V_S^2 = \mu_h - \frac{\sigma}{3K_h}\left(3K_h + 4\mu_h + 3m_h - \frac{1}{2}n_h\right), \tag{6b}$$

where V_P and V_S are the P- and S-wave velocities, ρ is the mass density of saturated rock, and l_h, m_h and n_h are stiff-pore 3oEC.

The acoustoelasticity theory provides the relationship between acoustic wave velocities and differential stress in saturated rocks at the high pressure range. However, the stress-induced non-linear variation of cracks and wave dispersion due to anelasticity are not accounted for in the classical acoustoelasticity theory. This has been proven to be a challenge as the experimental data on saturated rocks measured at a wide range of pressures and frequencies cannot be explained to-date.

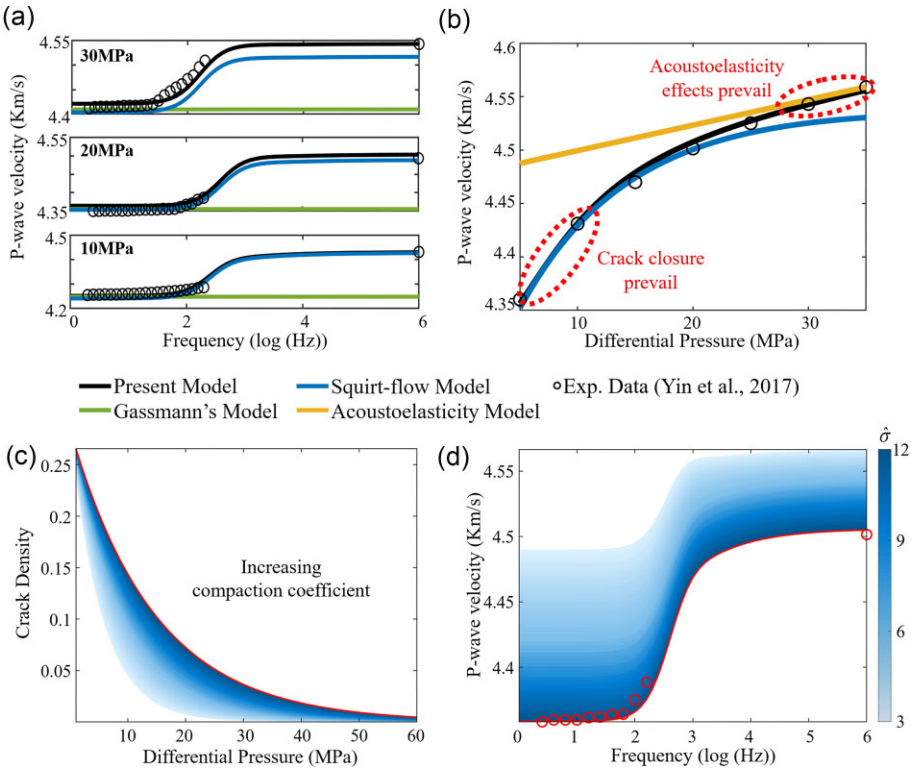

Figure 2. Comparison between the predictions of the Gassmann, squirt-flow and acoustoelasticity models and those of the present model with the experimental data of a brine -saturated sandstone (Yin *et al.* 2017) as a function of frequency (a); *P*-wave velocity (b) and crack density (c) as a function of differential pressure, and corresponding *P*-wave velocity dispersion for different compaction coefficients (d).

Table 1. Properties of the rock samples.

Sample	Lithology	Porosity (per cent)	Density ($kg\,m^{-3}$)	K_g (GPa)	μ_g (GPa)	Reference
A	Tight sandstone	8.93	2444	40.3	40.7	Yin *et al.* (2017)
B	Tight sandstone	3.77	2640	43.4	33.2	Han *et al.* (2021)
C	Carbonate	3.46	2734	75.3	42.9	This study
D	Shaly sandstone	21.00	2180	36.2	30.3	This study

2.2.2 *Frequency-dependent acoustoelasticity theory*

Since the microstructure in a saturated rock may be significantly influenced by stress (see Fig. 1), including stress-induced crack closure and enhanced grain-to-grain contact, the wave-induced fluid flow is affected as well. In analysing the combined effects of these mechanisms, the squirt-flow model is extended to include 3oEC.

According to eq. (6), the apparent bulk and shear moduli containing only stiff pores at hydrostatic pressure can be written as

$$K'_h = K_h - \frac{\sigma}{3K_h}\left(3K_h + 6l_h + \frac{2}{3}n_h\right), \tag{7a}$$

$$\mu'_h = \mu_h - \frac{\sigma}{3K_h}\left(3K_h + 4\mu_h + 3m_h - \frac{1}{2}n_h\right). \tag{7b}$$

The apparent double-porosity bulk (K'_m) and shear (μ'_m) moduli can be obtained from eq. (2).

$$K'_m = K'_h \Big/ \left(1 + \frac{16\left(1-(\nu'_h)^2\right)\rho_c}{9\,(1-2\nu'_h)}\right), \tag{8a}$$

$$\mu'_m = \mu'_h \Big/ \left(1 + \frac{32\,(1-\nu'_h)\,(5-\nu'_h)\,\rho_c}{45\,(2-\nu'_h)}\right), \tag{8b}$$

where $\nu'_h = (3K'_h - 2\mu'_h)/(6K'_h + 2\mu'_h)$ is the apparent Poisson ratio with only stiff pores.

By replacing the second-order moduli of eq. (1) with the apparent elastic moduli computed with eqs (7) and (8), the frequency-dependent equivalent 3oEC are

$$6l_{mf} + \frac{2}{3}n_{mf} = \frac{2K_{mf}^3}{\sigma}\left[\frac{1}{K'_h} - \frac{1}{K_{mf}} + \left(\left(\frac{1}{K'_m} - \frac{1}{K'_h}\right)^{-1} + \left(\left(\frac{1}{K_f^*} - \frac{1}{K_g}\right)\phi_c\right)^{-1}\right)^{-1}\right] - 3K_{mf}, \tag{9a}$$

$$3m_{mf} - \frac{1}{2}n_{mf} = \frac{2K_{mf}^3}{\sigma}\left[\frac{1}{\mu'_m} - \frac{1}{\mu_{mf}} - \frac{4}{15}\left(\frac{1}{K'_m} - \frac{1}{K_{mf}}\right)\right] - 3K_{mf} - 4\mu_{mf}. \tag{9b}$$

Then, by substituting eqs (1) and (9) into eq. (6), we obtain

$$\rho V_P^2 = \left(K_{mf} + \frac{4}{3}\mu_{mf}\right) - \frac{\sigma}{3K_{mf}}\left(7K_{mf} + \frac{16}{3}\mu_{mf} + 6l_{mf} + 4m_{mf}\right), \tag{10a}$$

$$\rho V_S^2 = \mu_{mf} - \frac{\sigma}{3K_{mf}}\left(3K_{mf} + 4\mu_{mf} + 3m_{mf} - \frac{1}{2}n_{mf}\right). \tag{10b}$$

3 MODELLING

The proposed model is applied to characterize the wave velocities in saturated rock in three steps. In the modelling, the elastic moduli

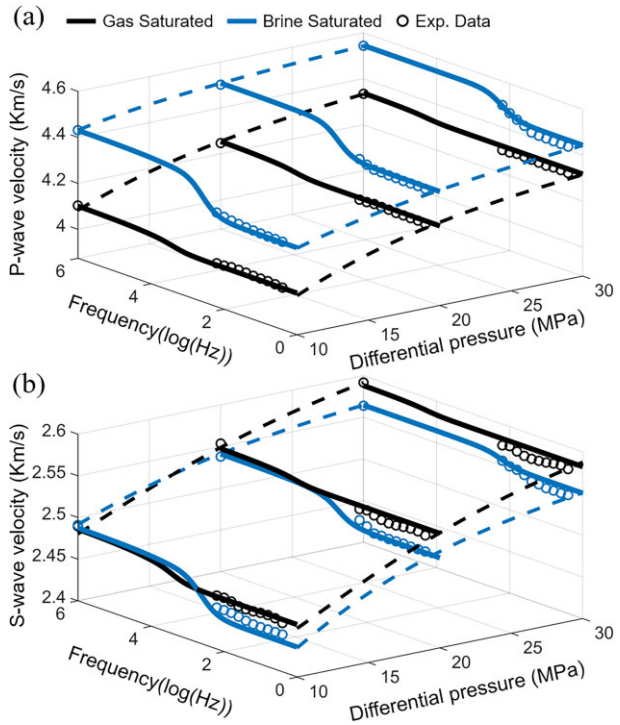

Figure 3. *P*-wave (a) and *S*-wave (b) velocities as a function of differential pressure and frequency for the tight sandstone sample A. The blue and black curves indicate the predictions for liquid- and gas-saturated states, respectively, and the circles are the measured data.

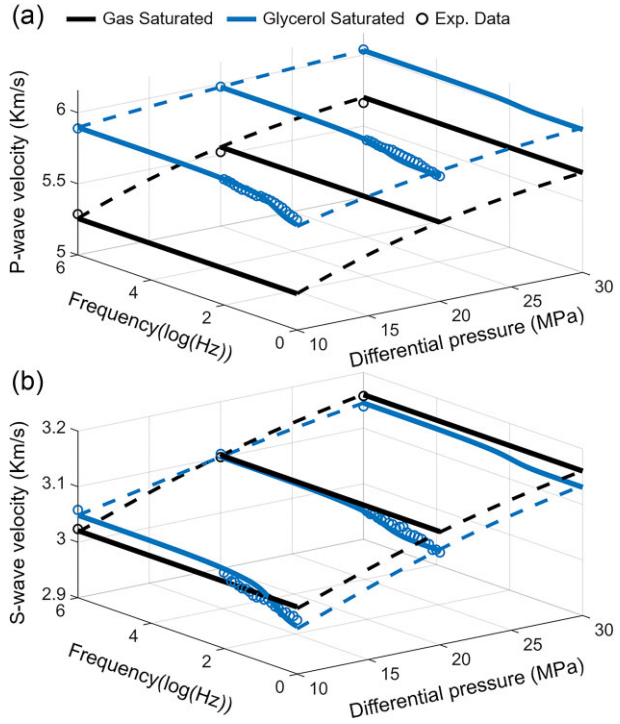

Figure 4. *P*-wave (a) and *S*-wave (b) velocities as a function of differential pressure and frequency for the tight sandstone sample B. The blue and black curves indicate the predictions for liquid- and gas-saturated states, respectively, and the circles are the measured data.

and crack parameters of dry/gas-saturated rock are estimated based on experimental velocities in the ultrasonic frequency range. For dry (or gas-saturated) conditions, the proposed model reduces to the conventional acoustoelasticity theory. Thus, the stiff moduli (K_h, μ_h, $6l_h + 2n_h/3$ and $3m_h - n_h/2$) can be estimated from the *P*- and *S*-wave velocities at high pressures. Then, K'_h and μ'_h are estimated with eq. (7). According to eqs (2) and (8), K_m, μ_m, K'_m and μ'_m can be determined with the crack density, and vice versa. The crack densities at different pressures are obtained by a least-squares fit to the dry-rock wave velocities. Moreover, $\hat{\sigma}$ and ρ_{ci} are obtained with eq. (3), and α_c and ϕ_c with eqs (4) and (5), respectively.

The crack parameters of the saturated rock in the ultrasonic frequency range are obtained. For the saturated state, the compressibility of cracks is almost equal to the pore fluid compressibility (David *et al.* 2013), which is related to the compaction coefficient $\hat{\sigma}$. For modelling the crack compressibility of the saturated rock, $\hat{\sigma}$ is obtained from the fully saturated rock velocities, and α_c and ϕ_c are estimated with eqs (4) and (5).

Finally, the frequency-dependent elastic moduli and wave velocities are obtained. By substituting the crack parameters and elastic moduli at ultrasonic frequencies into eqs (1) and (9), the frequency-dependent elastic constants (K_{mf}, μ_{mf}, $6l_{mf} + 2n_{mf}/3$ and $3m_{mf} - n_{mf}/2$) are obtained. These constants are then substituted into eq. (10) to obtain the frequency-dependent wave velocities.

Figs 2(a) and (b) compare the predictions of the proposed model, the Gassmann model (Gassmann 1951), the squirt-flow model, the classical acoustoelasticity model and the experimental data reported by Yin *et al*. (2017) for a sandstone under the brine-saturation condition. The properties of the sample are given in Table 1. The bulk modulus and viscosity of the brine are 2.28 GPa and 0.001 Pa·s, respectively. It is showed that the proposed model agrees with the squirt-flow model at low differential pressures (see the blue and black curves in Fig. 2b). This is because the second term on the right-hand side of eq. (10) is negligible at low pressures. At high differential pressures, the cracks tend to be closed and their parameters approach zero. Therefore, the proposed model reduces to the classical model of acoustoelasticity (see yellow and black curves in Fig. 2b). As $\hat{\sigma}$ increases, the crack density exhibits a weaker pressure dependence, implying stiffer cracks in the compression (Fig. 2c). The corresponding *P*-wave velocities for different compaction coefficients are given in Fig. 2(d).

4 RESULTS

4.1 Experiment

In this study, we measure *P*- and *S*-wave velocities at seismic and ultrasonic frequencies for a carbonate sample C and a shaly sandstone rock sample D. For the stress-strain measurements, the elastic modulus and Poisson's ratio are determined in the frequency range of 1–100 Hz with the forced oscillation method (Batzle *et al.* 2006; Yin *et al.* 2017). For the ultrasonic measurements, a pair of transducers is mounted in the aluminium caps at the ends of the specimens. The ultrasonic pulse transmission method (Birch 1960) is used to record waveforms and calculate velocities. Tests are performed at room temperature and differential pressures between 5 and 20 MPa. The pores are filled with nitrogen gas and water for a constant pore pressure of 1 MPa. Sample C is from the Longwangmiao Formation in the Gaoshiti-Moxi area, Sichuan Basin, China, which consists of

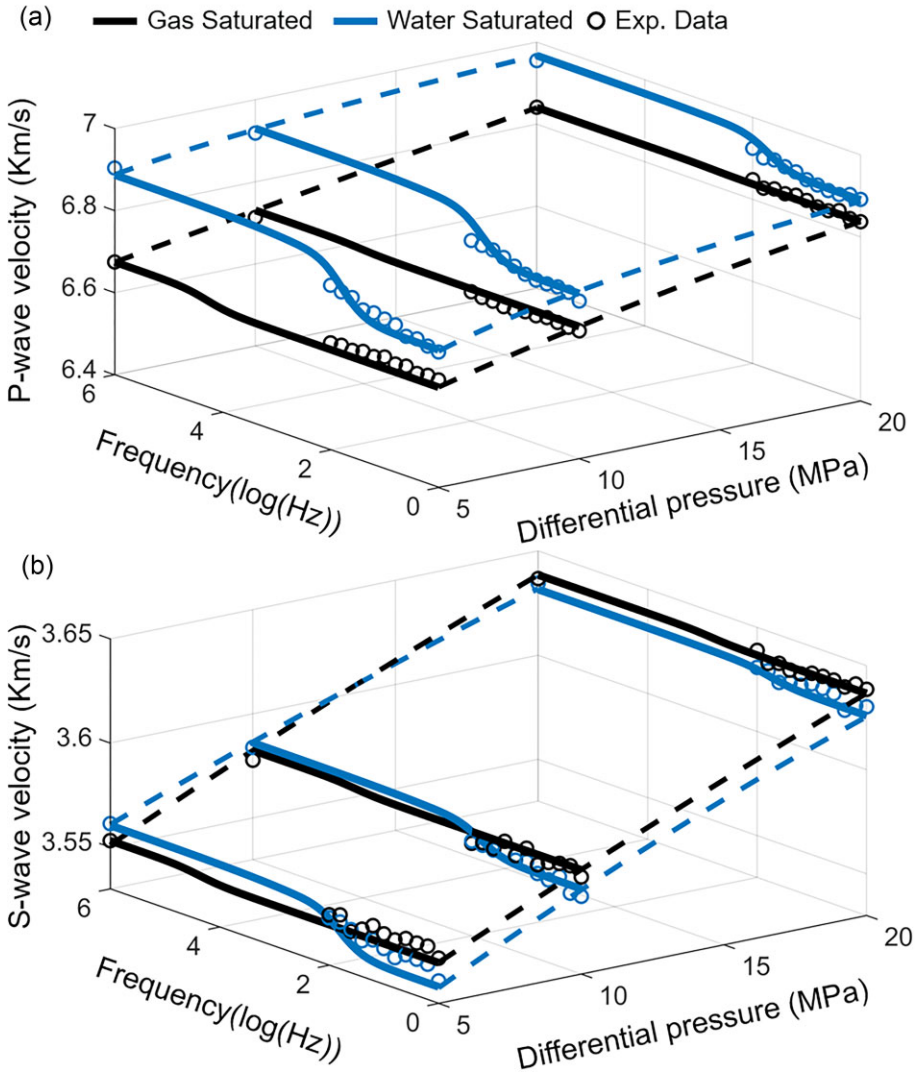

Figure 5. *P*-wave (a) and *S*-wave (b) velocities as a function of differential pressure and frequency for the carbonate sample C. The blue and black curves indicate the predictions for liquid- and gas-saturated states, respectively, and the circles are the measured data.

99.8 per cent calcite and has numerous isolated pores and intergranular dissolution pores connected by microcracks. Sample D is from a gas reservoir in the Jiyang Depression, East China, at about 2860 m depth. The rock mineral composition is quartz (70.37 per cent), clay (17.89 per cent), feldspar (6.55 per cent), dolomite (3.40 per cent) and siderite (1.8 per cent). Intergranular pores filled with clay minerals are developed.

We also predict the experimental wave velocities for samples from the literature. We consider the data for samples A and B reported by Yin *et al.* (2017) and Han *et al.* (2021), respectively (Table 1). Sample A (a tight sandstone) is mainly composed of quartz (78.4 per cent), feldspar (7.4 per cent), clay (5.45 per cent) and calcite (5.2 per cent), and the burial depth is 4458–4466 m. The grains are relatively compactly arranged, with visible long curves along the grain boundary dominating the connectivity of the pores. Crack porosity decreases from 0.023 to 0.001 per cent in the 0–35 MPa pressure range, and pore pressure is 1 MPa. Nitrogen gas and brine are used as pore fluids for the tests. Sample B (a tight sandstone) is mainly composed of quartz (40 per cent), feldspar (28 per cent), calcite (15 per cent), muscovite (12 per cent) and clay (5 per cent) with calcite fillings in the intergranular pores. The pore pressure is 1 MPa and the pore fluid of the saturated test is glycerol, whose bulk modulus and viscosity are 4.66 GPa and 0.86 Pa s, respectively. The differential pressures are set in the range of 0–50 MPa for the high-frequency measurement and 0–20 MPa at low frequencies.

4.2 Wave velocities versus stress and frequency

Figs 3–6 shows our model-predicted *P*- and *S*-wave velocities as a function of frequency and differential pressure, which agree with the experimental data of four samples. At low frequencies, the *P*-wave velocity in the gas-saturated state is lower than that with liquid. The trend of the *S*-wave velocity is opposite, which is due to the fact that shear modulus of the rock frame is constant with respect to different saturating fluids (Gassmann 1951), while the density of a liquid-saturated rock is higher than that at the gas-saturated state. The *P*- and *S*-wave velocities are only weakly frequency dependent in the gas-saturated state, while a significant dispersion is observed when the rocks are saturated with brine or glycerine. It is plausible that a fluid with lower mobility, such as brine or glycerol, tends to hinder fluid pressure gradient equilibrium/relaxation between pores

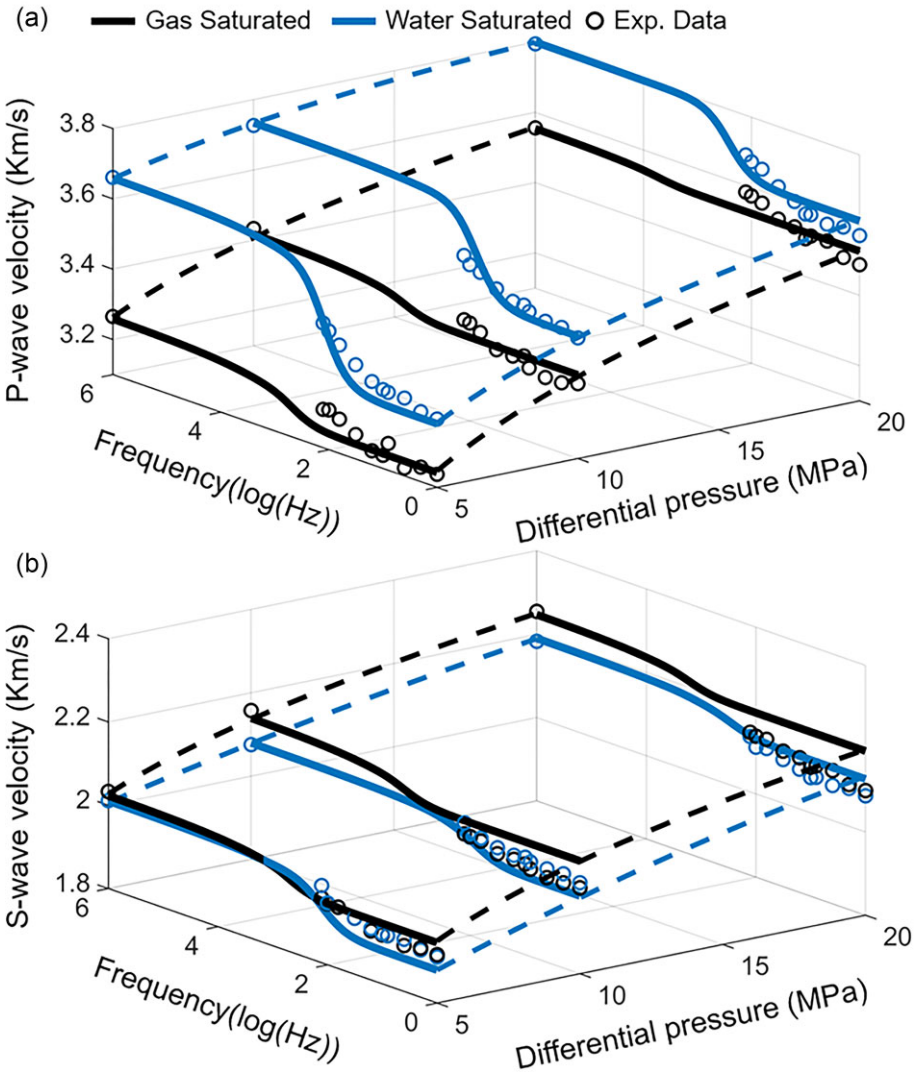

Figure 6. *P*-wave (a) and *S*-wave (b) velocities as a function of differential pressure and frequency for the shaly sandstone sample D. The blue and black curves indicate the predictions for liquid- and gas-saturated states, respectively, and the circles are the measured data.

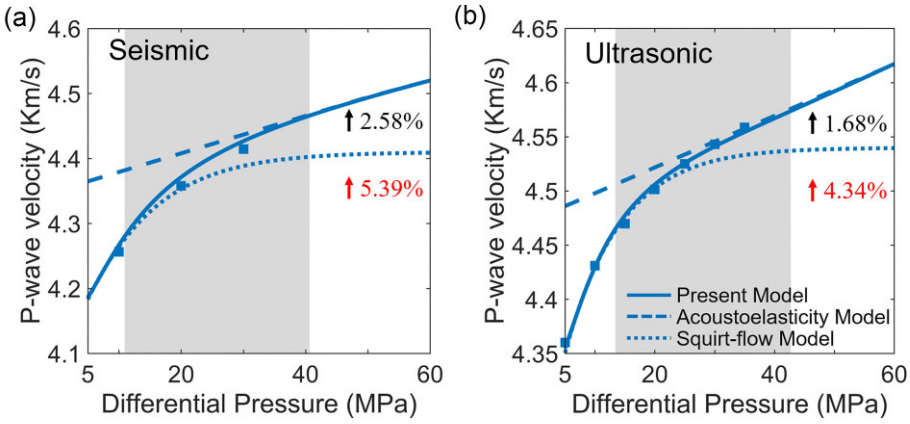

Figure 7. *P*-wave velocity as a function of differential pressure in the seismic (a) and ultrasonic regions (b) for the tight sandstone sample A, with the black and red arrows indicating the increase in velocity due to acoustoelasticity and crack closure, respectively.

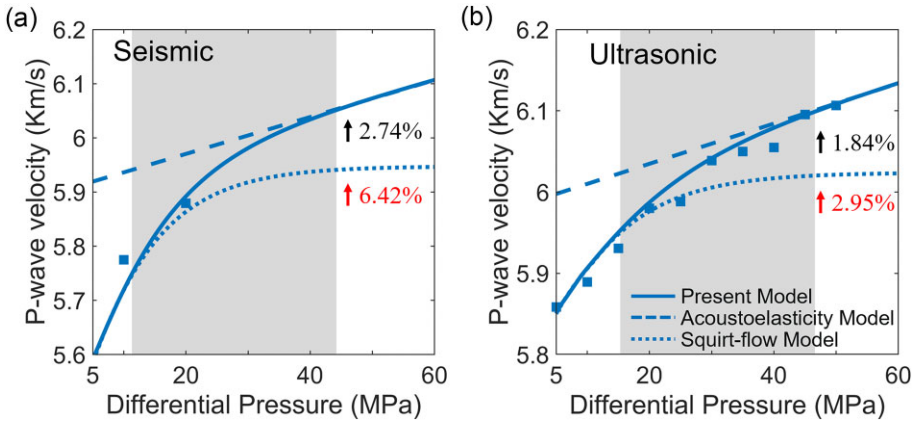

Figure 8. *P*-wave velocity as a function of differential pressure in the seismic (a) and ultrasonic regions (b) for the tight sandstone sample B, with the black and red arrows indicating the increase in velocity due to acoustoelasticity and crack closure, respectively.

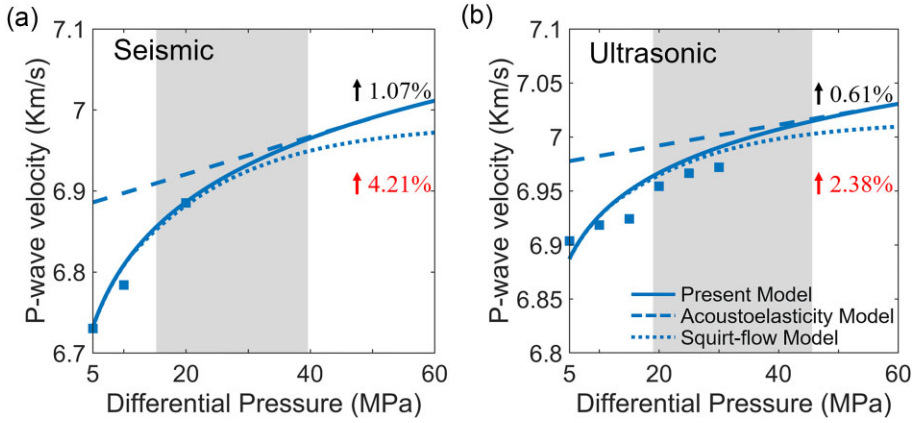

Figure 9. *P*-wave velocity as a function of differential pressure in the seismic (a) and ultrasonic regions (b) for the carbonate sample C, with the black and red arrows indicating the increase in velocity due to acoustoelasticity and crack closure, respectively.

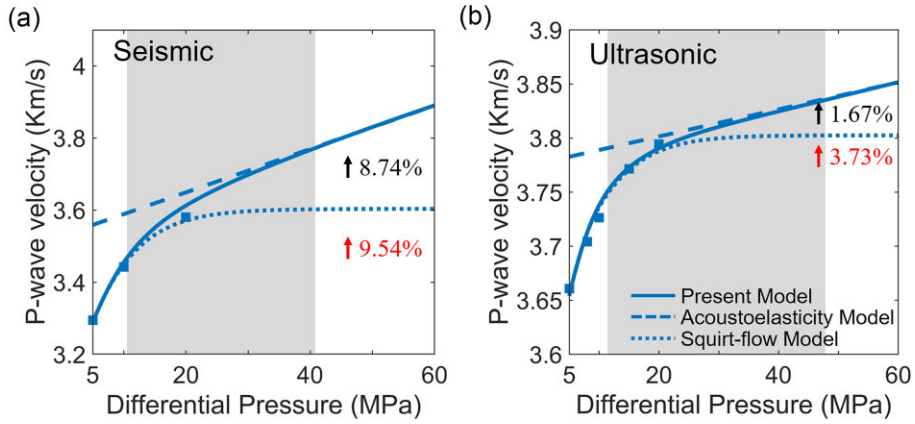

Figure 10. *P*-wave velocity as a function of differential pressure in the seismic (a) and ultrasonic regions (b) for the shaly sandstone sample D, with the black and red arrows indicating the increase in velocity due to acoustoelasticity and crack closure, respectively.

and cracks in the squirt-flow process, at the high frequency range (Mavko & Jizba 1991; Batzle *et al.* 2006). The dispersion decreases with increasing differential pressure due to crack closure and closer grain-to-grain contact.

The curves of *P*-wave velocity in the saturated state as a function of differential pressure are plotted at seismic and ultrasonic frequencies (Figs 7–10), which can be considered as three stages. In stage 1, the wave velocity increases non-linearly with pressure due to crack closure. In stage 2 (shaded areas in Figs 7–10), for the transition from a non-linear to a linear trend, the effects of acoustoelasticity appear. In stage 3, the effect of crack closure diminishes and acoustoelasticity predominates. At seismic frequencies, the pressure-induced velocity increase described by the squirt-flow model is responsible for the crack closure, while the discrepancies between the predictions of the squirt-flow model and the proposed model are considered as the acoustoelasticity effect. The crack closure

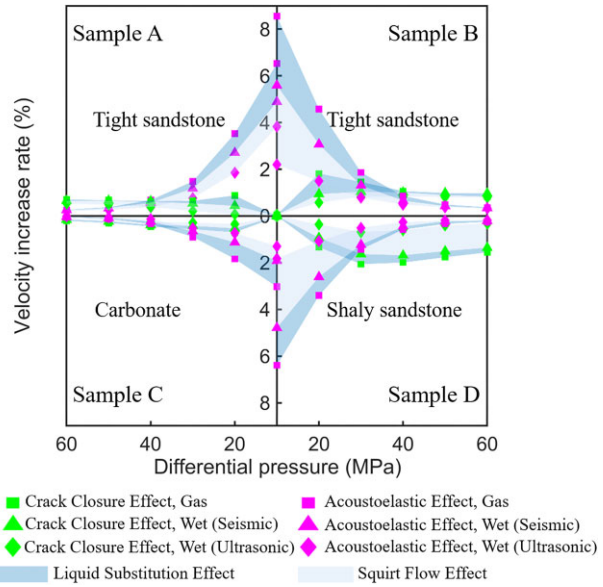

Figure 11. Effect of fluid properties, microstructure, and acoustoelasticity on the increase in *P*-wave velocity as a function of differential pressure in the four samples.

effects lead to an increase in *P*-wave velocity of 5.39, 6.42, 4.21 and 9.54 per cent for samples A, B, C and D, respectively, and the corresponding acoustoelasticity effects are 2.58, 2.74, 1.07 and 8.74 per cent, respectively, which are lowest for carbonate sample C. The effects are smaller at ultrasonic frequencies compared to seismic frequencies due to the squirt-flow effect and are 2.38–4.34 per cent and 0.61–1.84 per cent of the crack closure and acoustoelasticity effects, respectively.

4.3 Effects of the pore structure and fluid on wave velocities

Wave velocities are shown to exhibit strong frequency and pressure dependencies, the former related to squirt flow, particularly pronounced after liquid substitution, and the latter to stiffening effects due to crack closure and acoustoelasticity. The effects of these factors on the increase in *P*-wave velocity as a function of stress are quantified in Fig. 11. The green and red symbols represent the effects of crack closure and acoustoelasticity, respectively. The dark region between gas-saturated and liquid-saturated cases at the low frequencies represents the effects of liquid substitution (with the change in bulk modulus and density of the liquid), while the grey region between the low and high frequency regions at liquid-saturated states represents the effects of squirt flow. The effect of crack closure decreases with increasing pressure, and the strongest effect of acoustoelasticity occurs at about 20 MPa for samples A–C and 30 MPa for sample D.

In the low-pressure region, the pressure dependence of wave velocities is associated with cracks closure rather than acoustoelasticity. With increasing pressure, acoustoelasticity gradually takes the dominant role. The transition of samples A, B, C, and D occurs at pressures of 42, 37, 39 and 28 MPa, respectively. Sample D has the highest porosity and clay content, while sample C contains almost no clay and has the lowest porosity. The softening effect of clay (Clark *et al.* 1980) and the higher porosity make sample D more susceptible to compaction and cause the dominance of acoustoelasticity in a lower pressure range. As the cracks approach closure at the high pressure end, the squirt-flow effect disappears and the effect of fluid substitution is weakened. As a result, the velocity dispersion decreases.

The effects of crack closure and acoustoelasticity are smaller in the liquid-saturated state than in the dry/gas-saturated state at seismic frequencies. A plausible explanation could be that the liquid restricts the compressive deformation of cracks and grains (Khazanehdari & Sothcott 2003). These effects are even smaller at ultrasonic frequencies, which is due to the hydraulically isolated behaviour of the unrelaxed pore fluid (due to squirt flow). The effect of squirt flow is even more pronounced than that of fluid substitution.

The effects of fluid properties (sum of the effects of fluid substitution and squirt flow), microstructure, and acoustoelasticity are weaker in the carbonate sample C than in the sandstone samples. The maximum increases in wave velocity per 10 MPa reach 2.7, 6.5 and 1 per cent for sample A, 6.3, 8.5 and 1.5 per cent for sample B, and 4.6, 6.4 and 2.1 per cent for sample D due to those effects, respectively. In contrast, they only reach 1.7, 3.2 and 0.8 per cent for the carbonate sample C, which could be related to the lower sensitivity to differential stress due to the low crack content and tight grain contacts.

5 CONCLUSIONS

A frequency-dependent acoustoelasticity model is presented by extending the Gurevich's squirt-flow model with third-order elastic constants to characterize the combined effects of stress-induced non-linear deformation of cracks, finite deformation of grains, and pore fluid on acoustic wave responses. The model is consistent with the classical acoustoelasticity theory at high pressures. We perform seismic and ultrasonic measurements in carbonate and shaley sandstone samples as a function of differential pressures. In addition, a comparative analysis between the theoretical predictions and the measured data, as well as data published in the literature shows the strong frequency and pressure dependence of the wave velocities, which we can explain with the proposed model. The frequency dependence can be characterized by squirt flow, particularly pronounced after liquid substitution. While two mechanisms jointly explain the pressure-dependent velocities. Crack closure dominates the non-linear increase in wave velocities during the initial phase of loading. With increasing differential pressure, acoustoelasticity gradually approaches the main role.

How these effects affect the rate of increase in *P*-wave velocity are analysed. The rates of increase in velocity with respect to differential pressure due to fluid properties and crack closure decrease with differential pressure, while that of acoustoelasticity first increases and then decreases. The strong influence of acoustoelasticity occurs at 20–30 MPa and tends to dominate the velocity increase in the range of 28–44 MPa. The transition occurs at a lower pressure in clay-rich rock with higher porosity. At dry/gas-saturated conditions and seismic frequencies, the effects of crack closure and acoustoelasticity are strong, while at wet conditions and ultrasonic frequencies, a smaller fraction of the effects are observed. The pressure and frequency dependence of velocity is lower in the carbonate sample than in the sandstone sample, due to the low porosity. The present model can be applied to correlate laboratory measurements with well-log data and seismic field data to quantify the seismic velocities and elastic properties for a target formation in terms of *in situ* stress, providing a tool for inverting subsurface rock properties, evaluating reservoir quality and estimating fluid distribution.

ACKNOWLEDGMENTS

The authors gratefully acknowledge supports from the National Natural Science Foundation of China (grants nos. 41974123 and 42174161) and the Jiangsu Province Science Fund for Distinguished Young Scholars (grant no. BK20200021).

AUTHOR CONTRIBUTIONS

Conceptualization: Jing Ba; Data curation: Jing Ba, Genyang Tang, Yijun Wei; Formal analysis: Jing Ba, Yijun Wei, José M. Carcione, Ludmila Adam; Funding acquisition: Jing Ba; Investigation: Jing Ba, Yijun Wei; Methodology: Jing Ba, Yijun Wei, José M. Carcione; Project Administration: Jing Ba; Resources: Jing Ba; Software: Yijun Wei; Supervision: Jing Ba, José M. Carcione, Ludmila Adam; Validation: Jing Ba, Yijun Wei, José M. Carcione; Visualization: Yijun Wei; Writing – original draft: Jing Ba, Yijun Wei; Writing – review & editing: Jing Ba, Yijun Wei.

CONFLICTS OF INTEREST

The authors declare that they have no known competing financial interest or personal relationship that could have appeared to influence the work reported in this paper.

DATA AVAILABILITY

The experimental data and code of this study can be accessed at https://doi.org/10.5281/zenodo.8371594 and https://doi.org/10.5281/zenodo.8363060, respectively.

REFERENCES

Alkhimenkov, Y., Caspari, E., Gurevich, B., Barbosa, N.D., Glubokovskikh, S., Hunziker, J. & Quintal, B., 2020. Frequency-dependent attenuation and dispersion caused by squirt flow: three-dimensional numerical study. *Geophysics,* **85**(3), MR129–MR145.

Alkhimenkov, Y. & Quintal, B., 2022. An accurate analytical model for squirt flow in anisotropic porous rocks—Part 1: classical geometry. *Geophysics,* **87**(2), MR85–MR103.

Ba, J., Carcione, J.M., Cao, H., Yao, F. & Du, Q., 2013. Poro-acoustoelasticity of fluid-saturated rocks. *Geophys. Prospect.,* **61,** 599–612.

Batzle, M.L., Han, D.H. & Hofmann, R., 2006. Fluid mobility and frequency-dependent seismic velocity—direct measurements. *Geophysics,* **71**(1), N1–N9.

Biot, M.A., 1956. Theory of propagation of elastic waves in a fluid-saturated porous solid. II: higher frequency range. *J. acoust. Soc. Am.,* **28,** 179–191.

Biot, M.A., 1962. Mechanics of deformation and acoustic propagation in porous media. *J. appl. Phys.,* **33,** 1482–1498.

Biot, M.A., 1973. Nonlinear and semilinear rheology of porous solids. *J. geophys. Res.,* **78**(23), 4924–4937.

Birch, F., 1960. The velocity of compressional waves in rocks to 10 kilobars: 1. *J. geophys. Res.,* **65**(4), 1083–1102.

Brugger, K., 1964. Thermodynamic definition of higher order elastic coefficients. *Phys. Rev.,* **133,** A1611–A1612.

Carcione, J.M. & Gurevich, B., 2011. Differential form and numerical implementation of Biot's poroelasticity equations with squirt dissipation. *Geophysics,* **76,** N55–N64.

Chapman, S., Borgomano, J.V., Yin, H., Fortin, J. & Quintal, B., 2019. Forced oscillation measurements of seismic wave attenuation and stiffness moduli dispersion in glycerine-saturated Berea sandstone. *Geophys. Prospect.,* **67**(4), 956–968.

Chapman, S., Tisato, N., Quintal, B. & Holliger, K., 2016. Seismic attenuation in partially saturated Berea sandstone submitted to a range of confining pressures. *J. geophys. Res.,* **121,** 1664–1676.

Clark, V.A., Tittmann, B.R. & Spencer, T.W., 1980. Effect of volatiles on attenuation (Q^{-1}) and velocity in sedimentary rocks. *J. geophys. Res.,* **85**(B10), 5190–5198.

David, E.C., Fortin, J., Schubnel, A., Guéguen, Y. & Zimmerman, R.W., 2013. Laboratory measurements of low-and high-frequency elastic moduli in Fontainebleau sandstone. *Geophysics,* **78**(5), D369–D379.

David, E.C. & Zimmerman, R.W., 2012. Pore structure model for elastic wave velocities in fluid-saturated sandstones. *J. geophys. Res.,* **117**(B7), doi:10.1029/2012JB009195.

Dvorkin, J., Mavko, G. & Nur, A., 1995. Squirt flow in fully saturated rocks. *Geophysics,* **60**(1), 97–107.

Dvorkin, J. & Nur, A., 1993. Dynamic poroelasticity: a unified model with the squirt and the Biot mechanisms. *Geophysics,* **58**(4), 524–533.

Fu, B.Y. & Fu, L.Y., 2018. Poro-acoustoelasticity with compliant pores for fluid-saturated rocks. *Geophysics,* **83**(3), WC1–WC14.

Gassmann, F., 1951. Uber die elastizität poroser Medien. *Vierteljahrsschr. Naturforsch. Ges. Zurich,* **96,** 1–23.

Green, R.E., 1973. *Ultrasonic Investigation of Mechanical Properties, Treatise on Materials Science and Technology*. Academic Press.

Gurevich, B. & Carcione, J.M., 2022. *Attenuation and Dispersion of Elastic Waves in Porous Rocks: Mechanisms and Models,* Issue 26 of Geophysical references, Society of Exploration Geophysicists.

Gurevich, B., Makarynska, D., Paula, O.B.D. & Pervukhina, M., 2010. A simple model for squirt-flow dispersion and attenuation in fluid-saturated granular rocks. *Geophysics,* **75**(6), N109–N120.

Gurevich, B., Makarynska, D. & Pervukhina, M., 2009. Ultrasonic moduli for fluid-saturated rocks: Mavko-Jizba relations rederived and generalized. *Geophysics,* **74**(4), N25–N30.

Han, T., Liu, B. & Sun, J., 2018. Validating the theoretical model for squirt-flow attenuation in fluid saturated porous rocks based on the dual porosity concept. *Geophys. J. Int.,* **214**(3), 1800–1807.

Han, X., Wang, S., Tang, G., Dong, C., He, Y., Liu, T., Zhao, L. & Sun, C., 2021. Coupled effects of pressure and frequency on velocities of tight sandstones saturated with fluids: measurements and rock physics modelling. *Geophys. J. Int.,* **226**(2), 1308–1321.

Hughes, D. & Kelly, J., 1953. Second-order elastic deformation of solids. *Phys. Rev.,* **92**(5), 1145–1149.

Jones, G.L. & Kobett, D., 1963. Interaction of elastic waves in an isotropic solid. *J. acoust. Soc. Am.,* **35,** 5–10.

Khaksar, A., Griffiths, C.M. & McCann, C., 1999. Compressional- and shear-wave velocities as a function of confining stress in dry sandstones. *Geophys. Prospect.,* **47**(4), 487–508.

Khazanehdari, J. & Sothcott, J., 2003. Variation in dynamic elastic shear modulus of sandstone upon fluid saturation and substitution. *Geophysics,* **68**(2), 472–481.

Kravchishin, O.Z. & Chekurin, V.F.,(2009., Acoustoelasticity model of inhomogeneously deformed bodies. *Mech. Solids,* **44**(5), 781–791.

Lissa, S., Barbosa, N.D., Caspari, E., Alkhimenkov, Y. & Quintal, B., 2020. Squirt flow in cracks with rough walls. *J. geophys. Res.,* **125**(4), e2019JB019235.

Mavko, G. & Jizba, D., 1991. Estimating grain-scale fluid effects on velocity dispersion in rocks. *Geophysics,* **56**(12), 1940–1949.

Mavko, G. & Nur, A., 1975. Melt squirt in the asthenosphere. *J. geophys. Res.,* **80**(11), 1444–1448.

Mavko, G.M. & Nur, A., 1979. Wave attenuation in partially saturated rocks. *Geophysics,* **44**(2), 161–178.

Meegan, G.D., Johnson, P.A., Guyer, R.A. & McCall, K.R., 1993. Observations on nonlinear elastic wave behavior in sandstone. *J. acoust. Soc. Am.,* **94,** 3387–3391.

Mori, T. & Tanaka, K., 1973. Average stress in matrix and average elastic energy of materials with misfitting inclusions. *Acta Metall.,* **21**(5), 571–574.

Müller, T.M., Gurevich, B. & Lebedev, M., 2010. Seismic wave attenuation and dispersion resulting from wave-induced flow in porous rocks—a review. *Geophysics,* **75**(5), 75A147–75A164.

Murnaghan, F.D., 1937. Finite deformations of an elastic solid. *Am. J. Math.,* **59**(2), 235–260.

Murphy, W.F., 1982. Effects of partial water saturation on attenuation in Massilon sandstone and Vycor porous glass. *J. acoust. Soc. Am.,* **71**(6), 1458–1468.

Murphy, W.F., Winkler, K.W. & Kleinberg, R.L., 1986. Acoustic relaxation in sedimentary rocks: dependence on grain contacts and fluid saturation. *Geophysics,* **51**(3), 757–766.

Nur, A. & Simmons, G., 1969. Stress-induced velocity anisotropy in rock: an experimental study. *J. geophys. Res.,* **74**(27), 6667–6674.

Paula, O., Pervukhina, M., Makarynska, D. & Gurevich, B., 2012. Modeling squirt dispersion and attenuation in fluid-saturated rocks using pressure dependency of dry ultrasonic velocities. *Geophysics,* **77**(3), WA157–WA168.

Pimienta, L., Fortin, J. & Guéguen, Y., 2015a. Bulk modulus dispersion and attenuation in sandstones. *Geophysics,* **80**(2), D111–D127.

Pimienta, L., Fortin, J. & Guéguen, Y., 2015b. Experimental study of Young's modulus dispersion and attenuation in fully saturated sandstones. *Geophysics,* **80**(5), L57–L72.

Pimienta, L., Fortin, J. & Guéguen, Y., 2016. Effect of fluids and frequencies on Poisson's ratio of sandstone samples. *Geophysics,* **81**(2), D183–D195.

Pride, S.R. *et al.*, 2003. Permeability dependence of seismic amplitudes. *Leading Edge,* **22**(6), 518–525.

Pride, S.R., Berryman, J.G. & Harris, J.M., 2004. Seismic attenuation due to wave induced flow. *J. geophys. Res.,* **109**(B1), doi:10.1029/2003JB002639.

Shapiro, S.A., 2003. Elastic piezosensitivity of porous and fractured rocks. *Geophysics,* **68**(2), 482–486.

Shen, H., Li, X., Li, Q. & Wang, H., 2020. A method to model the effect of pre-existing cracks on P-wave velocity in rocks. *J. Rock Mech. Geotech. Eng.,* **12**(3), 493–506.

Smith, T., Sondergeld, C. & Tinni, A.O., 2010. Microstructural controls on electric and acoustic properties in tight gas sandstones; some empirical data and observations. *Leading Edge,* **29**(12), 1470–1474.

Tang, X., 2011. A unified theory for elastic wave propagation through porous media containing cracks—an extension of Biot's poroelastic wave theory. *Sci. China Earth Sci.,* **54,** 1441–1452.

Tisato, N., Madonna, C. & Saenger, E.H., 2021. Attenuation of seismic waves in partially saturated Berea sandstone as a function of frequency and confining pressure. *Front. Earth Sci.,* **9,** doi:10.3389/feart.2021.641177.

Vernik, L. & Kachanov, M., 2010. Modeling elastic properties of siliciclastic rocks. *Geophysics,* **75**(6), E171–E182.

Walsh, J.B., 1965. The effect of cracks on the compressibility of rock. *J. geophys. Res.,* **70**(2), 381–389.

Wang, X.Q., Schubnel, A., Fortin, J., David, E.C., Guéguen, Y. & Ge, H.K., 2012. High Vp/Vs ratio: saturated cracks or anisotropy effects? *Geophys. Res. Lett.,* **39**(11), doi:10.1029/2012GL051742.

Wang, Z. & Nur, A., 1990. Dispersion analysis of acoustic velocities in rocks. *J. acoust. Soc. Am.,* **87**(6), 2384–2395.

White, J.E., 1975. Computed seismic speeds and attenuation in rocks with partial gas saturation. *Geophysics,* **40**(2), 224–232.

Winkler, K.W., 1985. Dispersion analysis of velocity and attenuation in Berea sandstone. *J. geophys. Res.,* **90**(B8), 6793–6800.

Winkler, K.W. & Liu, X., 1996. Measurements of third-order elastic constants in rocks. *J. acoust. Soc. Am.,* **100,** 1392–1398.

Winkler, K.W. & McGowan, L., 2004. Nonlinear acoustoelastic constants of dry and saturated rocks. *J. geophys. Res.,* **109**(B10), doi:10.1029/2004JB003262.

Wyllie, M.R.J., Gregory, A.R. & Gardner, G.H.F., 1958. An experimental investigation of factors affecting elastic wave velocities in porous media. *Geophysics,* **23,** 459–493.

Yin, H., Zhao, J., Tang, G., Zhao, L., Ma, X. & Wang, S., 2017. Pressure and fluid effect on frequency-dependent elastic moduli in fully saturated tight sandstone. *J. geophys. Res.,* **122**(11), 8925–8942.